Discrete Layer Jamming for Safe Co-Robots

Yitong Zhou, Leon M. Headings, and Marcelo J. Dapino

Abstract— **High injury severity occurs when a stiff robot arm hits an operator. Introducing compliance into robot systems reduces the impact and enables safe interaction, but at the expense of positioning performance and payload capacity. This paper presents a tunable stiffness mechanism for safe human-robot interaction based on discrete layer jamming. The proposed design of a discrete layer jamming mechanism is a robot link made of multiple thin layers of ABS and multiple clamps. By applying high clamping pressure to the laminates, the link behaves like a rigid link; reducing the clamping pressure softens the link which yields safer human-robot interaction. Compared to conventional pneumatic layer jamming, discrete layer jamming allows for simplicity of installation with dynamic actuators, faster control, greater portability since no air supply is needed, and no sealing issues. To validate the concept, this paper investigates a discrete layer jamming beam made of ten ABS laminates and two aluminum clamps that cover 10% of the surface of the beam. Stiffness tests have been performed, showing that around 17 times bending stiffness change is achieved by increasing the clamping pressure of two clamps from 0 to 1 MPa.**

I. Introduction

Collaborative robots (co-robots) work closely with human operators in a variety of applications such as exoskeletons for human strength amplification [1], wearable haptic devices [2], rehabilitation [3], [4], and flexible production lines [5]. Compared to conventional robots which are usually confined in cages and fences to ensure safety, co-robots are expected to be intrinsically safe such that humans interacting with them do not suffer injury.

In recent times, introducing controllable compliance into robotic systems has been proposed to fulfill safety requirements. A number of studies have shown that variable stiffness helps to achieve high performance safely. There are two representative mechanisms for varying stiffness: variable stiffness joints (VSJ) and variable stiffness links (VSL). As the first solution to be investigated, a large number of VSJ studies have been conducted [6]–[10]. The main research activities have been focusing on the safe brachistochrone problem, which is an optimal control problem of minimizing the time needed to move a mechanical load from one position to another under certain safety constraints. Head injury criterion (HIC) [11] has been widely used as a head injury indicator as well as a safety constraint in the robotics community [7], [9], [12].

Recent research has indicated an increasing interest in variable stiffness links. Various approaches have been investigated to achieve controllable stiffness. She et al. [13] proposed a variable stiffness parallel-guided link based on controlling the area moment of inertia of the cross sectional area of a robot arm. However, the stiffness ratio of 3.6 provides only a modest opportunity for improving performance while maintaining a safe HIC value. Stilli et al. [14] designed a controllable-stiffness robot link made of an airtight chamber formed by a plastic mesh and silicone wall; stiffness is varied by controlling the air pressure inside the chamber. However, the stiffness change capability is unclear because the stiffness at lower pressure states was not investigated.

Granular jamming using granular media has been investigated for robotic applications such as robotic spines [15] and gripping [16]. In another case, if a robotic link is composed of a volume of granular material, e.g. dry sand or coffee, it can effectively transition between compliant states and load-bearing stiff states by applying a vacuum to achieve variable stiffness [17], [18]. However, it requires a substantial volume to achieve sufficient stiffness which adds bulk to robotic manipulators.

A layer jamming system makes use of friction generated between flexible laminates by applying a jamming force to transition between soft and stiff states. A variety of methods have been implemented to provide a jamming force. Henke et al. [19] proposed a variable stiffness beam that uses an array of shape memory alloy (SMA) wires wrapped around a stack of laminates. By changing the temperature generated by an electrical current flowing through the SMA wires, the wires can contract or elongate, which changes the compression force around the layers, hence varying stiffness. However, this method is limited by the strength and speed of the SMA wires, and high SMA temperature on the outer surface may present a hazard. Tabata et al. [20] utilized electrostatic attractive forces generated by applying high voltage to flexible polyamide thin films with patterned nickel electrodes to change stiffness. However, high voltages used (from 150 V to 750 V) could be dangerous and the stiffness change is insufficient (4 times). A common approach, which uses a vacuum to generate the jamming force, has been investigated for a variety of applications including continuum robots [21], user interfaces for human-computer interaction [22], and minimally invasive surgery [23]. However, it requires an external vacuum source which adds complexity, bulk, and weight to the layer jamming system. Furthermore, the thin membranes used to contain the laminates are susceptible to damage from contact with rough edges.

In this paper, we propose a novel concept to change effective bending stiffness termed “discrete layer jamming.”

This research was supported by the National Science Foundation, Grant No: CMMI-1637656.

The authors are with the Department of Mechanical and Aerospace Engineering, The Ohio State University, Columbus, OH 43210 USA (e-mail:zhou.1455@osu.edu; headings.4@osu.edu; dapino.1@osu.edu).

Our proposed design incorporates variable pressure clamps at discrete locations along a multilayered flexible beam. The stiffness of the multilayered beam can be varied by changing the clamping pressure. For proof of concept, a ten-layered ABS beam with two aluminum mechanical clamps has been designed and tested for a range of clamping pressures. The article is organized as follows: the design purpose and concepts are presented in Section II. Section III shows the discrete layer jamming design, and experiments to evaluate the bending stiffness. Section IV provides a summary of the study and future work.

II. Design Purpose and Concepts

A. Safety Criterion

A typical free impact between a single robot arm and an operator is shown in Fig. 1(a). The robot arm is composed of an end effector with a load at one end and a link that is connected to a joint at the other end. The robot link has a length L and a mass m_{rob}. The end load is m_{load}. The operator's head with a mass denoted as m_{oper} is hit by the link at a distance r from the joint with an angular velocity ω. The velocity of the robot link at the impact location r is calculated as $v = \omega r$. The effective mass of the robot is m_{eff}, which is obtained by equating the kinetic energy of the mass m_{eff} and that of the original flexible vibrating beam, as shown in [24]. The effective bending stiffness of the link and the covering material of both the operator's head and the robot is k_{eff}. A mass-spring-mass impact model, shown in Fig. 1(b), was proposed by Bicchi et al. [7]. In their model, robot rotor and link are both considered as rigid, and the only compliance during impact is from the covering material. Hence, the HIC formula shown in Equation (1) of [7] is expressed as a function of robot covering material stiffness, robot inertia, and operator inertia. She et al. [12] modified the HIC equation for compliant link robots, replacing the covering material stiffness in [7] with an effective stiffness which is a resulting term of joint stiffness, link stiffness, and robot covering material stiffness. For a short impact period of T, the HIC is expressed as follows [7]:

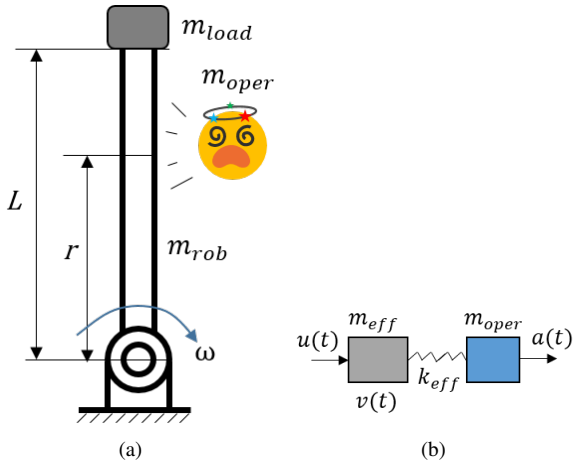

Fig. 1: (a) Human robot collision. (b) Mass-spring-mass model.

$$HIC = 1.016 T k_{eff}^{0.75} \frac{m_{oper}^{-0.75} m_{eff}^{1.75}}{(m_{eff} + m_{oper})^{1.75}} v^{2.5}, \quad (1)$$

which shows that HIC is affected by time duration of the impact, impact velocity, effective stiffness, effective mass, and operator's head mass. An HIC value of 100 may be considered as an appropriate threshold for human robot interaction [7]. To simplify and consider only the effect of a compliant link, joint stiffness and covering material stiffness can be reasonably assumed infinitely large, and the effective stiffness is simply the link stiffness $k_{eff} = 3YI/r^3$, where Y is the elastic modulus and I is the area moment of inertia of the link [12]. Substituting the link effective stiffness and $v = \omega r$ into (1) yields:

$$HIC(r) = 1.016 T (3YI)^{0.75} \frac{m_{oper}^{-0.75} m_{eff}^{1.75}}{(m_{eff} + m_{oper})^{1.75}} \omega^{2.5} r^{0.25}, \quad (2)$$

which shows that HIC increases with YI, angular velocity, impact length, and impact system masses. Fixing other parameters, when $r = L$, HIC is found to be maximum. Substituting $r = L$ into (2), HIC at L can be calculated as:

$$HIC(L) = 1.016 T \left(\frac{3YI}{L^3}\right)^{0.75} \frac{m_{oper}^{-0.75} m_{eff}^{1.75}}{(m_{eff} + m_{oper})^{1.75}} (\omega L)^{2.5}. \quad (3)$$

Here, $3YI/L^3$ is the bending stiffness of an Euler-Bernoulli beam for small deflections. It shows that the value of HIC increases with bending stiffness to the power of 0.75. Reducing bending stiffness helps to reduce the HIC value, hence improving safety. For instance, fixing other parameters and decreasing the bending stiffness by 10 times, the HIC value can be reduced by 5.6 times.

B. Layer Jamming Concept

The layer jamming concept is illustrated in Fig. 2, where the main structure is a multilayered beam. The most compliant state is shown in Fig. 2(a), where no compression force is applied and each layer bends almost independently when an end load is applied. A stiff state with external compression force applied to the outer surface of the beam is displayed in Fig. 2(b).

The compression force increases the friction coupling between the layers during bending to resist sliding and thus increases bending stiffness. The theoretical maximum stiffness change that a layer jamming system can achieve is n^2, where n represents the number of layers [19], [25]. Therefore, a 10-layered beam at its stiffest (fully jammed) state can theoretically be 100 times stiffer than its most compliant (unjammed) state. However, pneumatic layer jamming is limited by the capabilities of the pneumatic source and the actuation speed can be too slow for some types of robotic control.

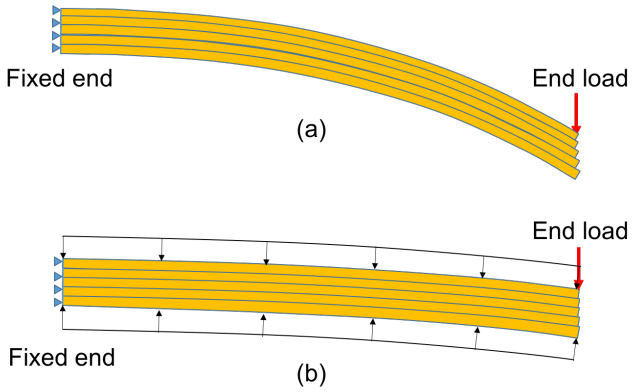

Fig. 2: Layer jamming concept. (a) Most compliant state. (b) Stiff state.

C. Discrete Layer Jamming Concept

Discrete layer jamming simplifies the variable pressure actuation system with variable pressure clamps as shown in Fig. 3. Instead of a pneumatic-based jamming force which requires a vacuum, a mechanical jamming force is applied by active clamps. By applying compression forces with discrete clamps to the outer surface of the beam, the bending stiffness of the beam can be significantly increased. The whole beam has a length of L and a width of W. Defining the number of laminates as n and the thickness of each laminate as t, the thickness of the beam is therefore $T = nt$. The whole length is then divided by two clamps into two segments of length L_1 and L_2, where $L_1 = L_2$ for simplicity. The two clamps have the same width so $C_1 = C_2$. Pressures P_1 and P_2 are applied to clamp 1 and clamp 2, respectively.

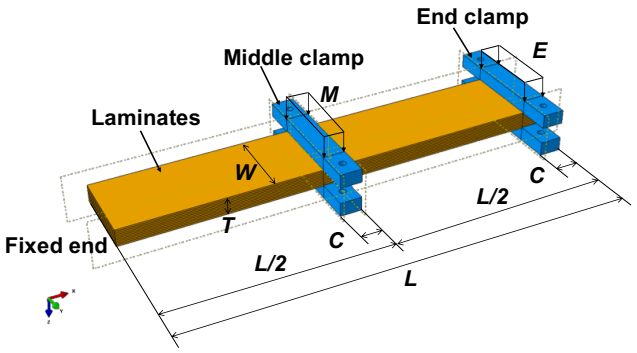

Fig. 3: Concept of discrete layer jamming.

Defining the number of clamps as N, and the friction coefficient as μ, the ith clamping force CF_i can be calculated as follows:

$$CF_i = P_i C_i W, \ i = 1, 2. \tag{4}$$

Therefore, the friction force F_i between all laminates at the ith clamp can be calculated as:

$$F_i = (n-1)\mu P_i C_i W, \ i = 1, 2. \tag{5}$$

TABLE I: Specifications and test conditions for experiments.

Symbol	Specification	Value
P_i	ith clamp pressure	0, 0.05, 0.5, 1, 3 MPa
W	Width of laminates	70 mm
t	Thickness of each laminate	1.5875 mm (1/16 in)
C_i	Width of ith clamp	20 mm, $i = 1, 2$
L_i	Length of ith segment	200 mm, $i = 1, 2$
n	The number of laminates	10
N	The number of clamps	2
μ	Friction coefficient	0.6
D	Tip deflection	40 mm
Y	Elastic modulus	2.2 GPa

The friction force from all clamps is simply:

$$F = \sum_{i=1}^{N} (n-1)\mu P_i C_i W, \ N = 1, 2. \tag{6}$$

Equation (6) indicates that the friction force from all clamps depends on the number of laminates, the clamp size, the friction coefficient, the clamping pressure, and the number of clamps. Since the friction force provides the sliding resistance, the higher the friction force, the more difficult it is for laminates to slide, and the higher the bending stiffness of the structure. Therefore, assuming a two-clamp system with fixed number of laminates, laminate dimensions, clamping area, and friction coefficients, the bending stiffness can be increased by increasing the clamp pressures P_1 and P_2. However, with fixed total thickness of the laminates, clamping area, friction coefficients, and clamping pressures, the bending stiffness can be decreased by increasing the number of laminates, since the stiffness of each laminate decreases in the third order of thickness. In order to investigate the effects of clamp pressures on the bending stiffness, in this paper we fix the number of laminates, laminate dimensions, clamping area, and friction coefficients.

III. Discrete Layer Jamming Experimental Validation

A. Prototype and Experimental Setup

To prove the discrete layer jamming concept, a 10-layered ABS stack was fabricated for testing. Each layer is 70 mm wide, 400 mm long, and 1.59 mm thick, for a total thickness of 15.9 mm. ABS was chosen for the test beam due to its flexibility. The layers were laser-cut to form the desired shape. Aluminum mechanical clamps were fabricated and assembled as shown in Fig. 4. Each clamp has a width of 20 mm. To quantify the pressure level, an Omega LC703-1k load cell is embedded into each clamp. Pressure is applied to the load cell by a pressure adjustment bolt at one end. The other end of the load cell is bolted to the pressing plate, which compresses the laminates. The applied clamping force can be increased by tightening the pressure adjustment bolt.

Quasi-static cantilever bending tests were set up and performed to evaluate the stiffness of the prototype for different levels of clamp pressure. Fig. 5 displays the test setup and Table I shows the prototype and test specifications.

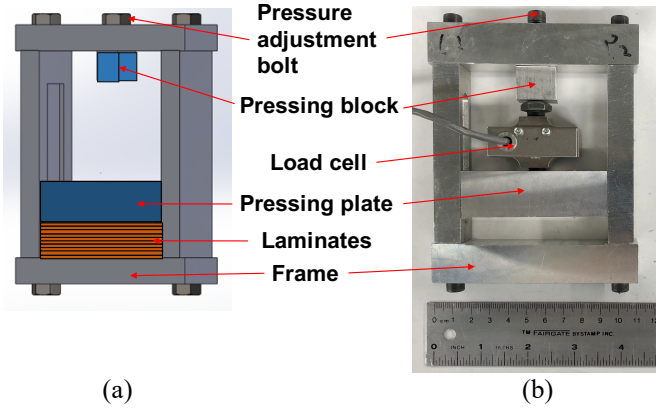

Fig. 4: Clamp design. (a) Solid rendering. (b) Experimental unit.

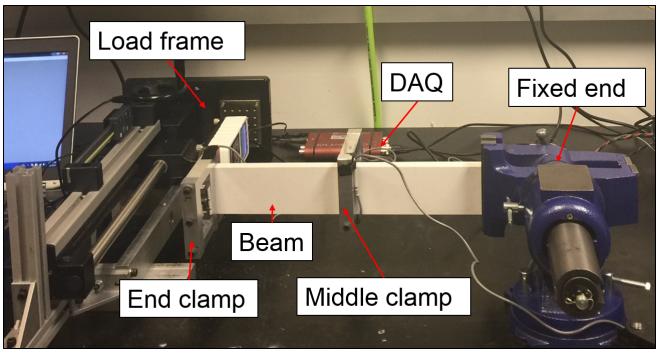

Fig. 5: Cantilever bending test setup.

The prototype was clamped at one end and deflected manually at the other end by a Mark-10 ES30 load frame. The first and second clamps were placed 180 mm and 380 mm from the fixed end, respectively, so that the beam length was equally partitioned into two segments. The tip load and tip deflection were measured by a Mark-10 ME-200 force gauge and a Mark-10 ESM001 digital travel display, respectively. To indicate the clamp location more clearly, the first and second clamp are named as the middle and end clamp, respectively.

B. Test Procedures

Twenty-five pressure states were set up and tested with pressure combinations of 0, 0.05, 0.5, 1, and 3 MPa applied to the middle and end clamps. Zero pressure throughout this paper means no pressure and no clamps, indicating the beam is free of constraints in clamped regions at the zero pressure state.

For each pressure state, one cantilever bending test was performed for three loading and unloading cycles. The tip was deflected to 40 mm for each loading cycle. For abbreviated notation of different pressure states, the pressure for middle and end clamps are denoted as "M_E_", where "M_" denotes the middle clamp pressure and "E_" denotes the end clamp pressure. The pressure unit throughout this paper is MPa. For example, M0E3 represents a pressure state with middle clamp pressure of 0 (no clamps and pressure) and end clamp pressure of 3 MPa. M0E0 represents the clamp and pressure free state.

C. Experimental Results and Discussion

The force-displacement curves are shown in Fig. 6 for M0, M0.05, M0.5, M1, and M3 cases with end clamp pressures of E0, E0.05, E0.5, E1, and E3. All figures except the M0 series exhibit similar slopes at very small deflections, which indicates that the stiffness is independent of the clamp pressure. This independence is due to the fact that slipping (laminates sliding relative to each other) occurs only when the shear force between individual laminates exceeds the limit for static friction. Below this level, the laminates effectively stick to each other. Once the laminates begin to slip, the curves become nonlinear. Fig. 6 (c), Fig. 6 (d), and Fig. 6 (e) look similar, which indicates that increasing middle clamp pressure above 0.5 MPa helps little to increase stiffness. The E0.5, E1, and E3 curves almost overlap with each other for every middle clamp pressure for the first part of the loading curve for the first cycle, thus providing similar stiffnesses. The M0E0.05 curve in Fig. 6(b) exhibits a wavy behavior at large deflection, and M1E0.05 and M3E0.05 curves both exhibit a drop, which are due to slipping between the laminates. Hysteresis was observed at all pressure states, but lower pressure states exhibit higher hysteresis. Hysteresis is likely a result of internal friction during sliding between the laminates; because there is less sliding at higher pressure states, there is less hysteresis.

To compare the overall stiffness of different pressure states, stiffness was calculated by fitting the slope of the first 20 mm of each force-displacement curve. Fig. 7 illustrates the stiffness versus end clamp pressure for different middle clamp pressures. While the overall trends of the curves show that higher end clamp pressures yield higher stiffnesses, the stiffness increases little when increasing end clamp pressure from 0.5 MPa to 3 MPa as we already observed in the force-displacement curves. Similarly, stiffness increases with middle clamp pressure and differs little at higher middle clamp pressures, i.e., M0.5, M1, and M3. The M0.05 curve shows a downward trend. The reason is that 0.05 MPa corresponds to a small load relative to the 3.17 MPa range of the load cell. Both clamps were adjusted between tests, which resulted in some variability in the applied pressures, especially for small pressures, i.e., the M0.05 series.

TABLE II: Stiffness for different middle and end clamp pressure combinations from experiments.

Stiffness (N/mm)		Middle clamp pressure (MPa)				
		0	0.05	0.5	1	3
End clamp pressure (MPa)	0	0.024	0.12	0.17	0.17	0.17
	0.05	0.10	0.19	0.35	0.34	0.36
	0.5	0.11	0.22	0.39	0.40	0.40
	1	0.12	0.22	0.40	0.40	0.41
	3	0.11	0.19	0.39	0.39	0.40

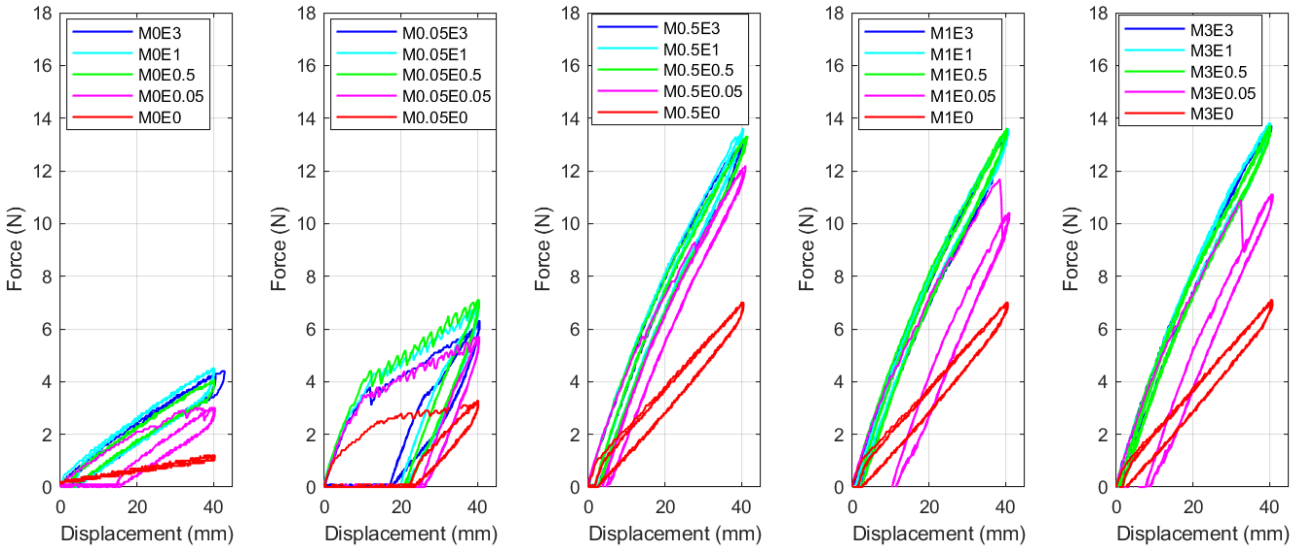

Fig. 6: Force-displacement curves of different pressure states. (a) M0 series tests. (b) M0.05 series tests. (c) M0.5 series tests. (d) M1 series tests. (e) M3 series tests.

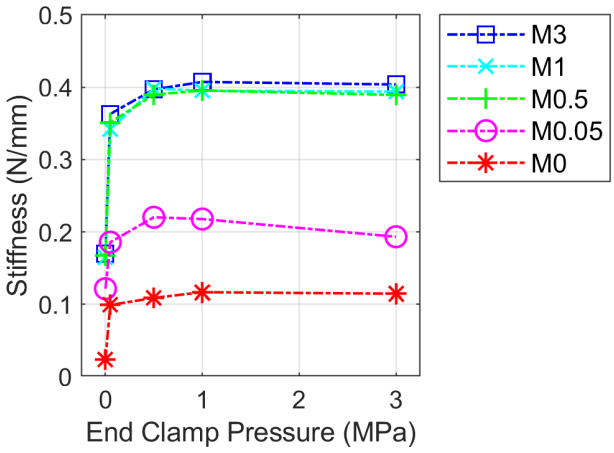

Fig. 7: Stiffness vs. end clamp pressure from experiments.

Stiffness ratio is defined as k_p/k_{min}, where k_p is the stiffness of a certain pressure state, and k_{min} is the minimum stiffness, corresponding to the case of no clamps or pressure. The maximum stiffness ratio is defined as $K_r = k_{max}/k_{min}$, where k_{max} is the maximum stiffness over the range of pressures investigated. Table II and Table III list the stiffnesses and stiffness ratios for all 25 pressure states. Here k_{max} was found to be 0.41 N/mm at the M3E1 pressure state and k_{min} 0.024 N/mm at the no clamp or pressure state (M0E0). The maximum stiffness ratio K_r is 17, which means that clamping two discrete clamps can provide a 17 times increase in bending stiffness. In addition, when comparing the stiffness on the opposite sides of the diagonal connecting M0E0 and M3E3 of Table II, e.g., M3E0.05 and M0.05E3, which are 0.36 N/mm and 0.19 N/mm respectively, it is observed that the upper right values are greater than the lower left values. Likewise, comparing the M0 column with the E0 row indicates that the middle clamp is more effective at increasing stiffness than the end clamp.

TABLE III: Stiffness ratio for different middle and end clamp pressure combinations from experiments.

Stiffness ratio		Middle clamp pressure (MPa)				
		0	0.05	0.5	1	3
End clamp pressure (MPa)	0	1.0	5.1	7.1	7.0	7.2
	0.05	4.2	7.9	15	14	15
	0.5	4.6	9.3	16	17	17
	1	4.9	9.2	17	17	17
	3	4.8	8.2	16	17	17

IV. Conclusions

This paper presented the principle of discrete layer jamming for tunable stiffness robot links, along with details of the design concept, prototype, and experimental results. Detailed analysis of its stiffness properties and verification of its performance based on experiments proved that beam stiffness increases with clamp pressure. The stiffness change of the current discrete layer jamming structure can be as high as 17 times, which makes discrete layer jamming structures promising for robotic applications.

Future work will focus on clamp actuator design and control to maximize safety and performance. The use of smart materials such as piezoelectrics will be considered due to their fast response. The design of automated clamping actuators will be an extension of the current work to be tackled in subsequent papers. There are a number of options ranging from conventional electrical actuators to shape

memory alloys. We will also investigate design parameters that affect bending stiffness, such as the number of clamps and clamp location.

REFERENCES

[1] A. Chu, H. Kazerooni, and A. Zoss, "On the biomimetic design of the berkeley lower extremity exoskeleton (bleex)," in *Robotics and Automation, 2005. ICRA 2005. Proceedings of the 2005 IEEE International Conference on*. Citeseer, 2005, pp. 4345–4352.

[2] A. Frisoli, F. Rocchi, S. Marcheschi, A. Dettori, F. Salsedo, and M. Bergamasco, "A new force-feedback arm exoskeleton for haptic interaction in virtual environments," in *Eurohaptics Conference, 2005 and Symposium on Haptic Interfaces for Virtual Environment and Teleoperator Systems, 2005. World Haptics 2005. First Joint*. IEEE, 2005, pp. 195–201.

[3] S. Roderick and C. Carignan, "Designing safety-critical rehabilitation robots," in *Rehabilitation Robotics*. InTech, 2007.

[4] E. T. Wolbrecht, V. Chan, D. J. Reinkensmeyer, and J. E. Bobrow, "Optimizing compliant, model-based robotic assistance to promote neurorehabilitation," *IEEE Transactions on Neural Systems and Rehabilitation Engineering*, vol. 16, no. 3, pp. 286–297, 2008.

[5] J. Krüger, T. K. Lien, and A. Verl, "Cooperation of human and machines in assembly lines," *CIRP Annals-Manufacturing Technology*, vol. 58, no. 2, pp. 628–646, 2009.

[6] A. Bicchi, G. Tonietti, and E. Piaggio, "Design, realization and control of soft robot arms for intrinsically safe interaction with humans," in *Proc. IARP/RAS Workshop on Technical Challenges for Dependable Robots in Human Environments*, 2002, pp. 79–87.

[7] A. Bicchi and G. Tonietti, "Fast and" soft-arm" tactics [robot arm design]," *IEEE Robotics & Automation Magazine*, vol. 11, no. 2, pp. 22–33, 2004.

[8] G. Tonietti, R. Schiavi, and A. Bicchi, "Optimal mechanical/control design for safe and fast robotics," in *Experimental Robotics IX*. Springer, 2006, pp. 311–320.

[9] S. Haddadin, A. Albu-Schäffer, O. Eiberger, and G. Hirzinger, "New insights concerning intrinsic joint elasticity for safety," in *Intelligent Robots and Systems (IROS), 2010 IEEE/RSJ International Conference on*. IEEE, 2010, pp. 2181–2187.

[10] L. Chen, M. Garabini, M. Laffranchi, N. Kashiri, N. G. Tsagarakis, A. Bicchi, and D. G. Caldwell, "Optimal control for maximizing velocity of the compact™ compliant actuator," in *Robotics and Automation (ICRA), 2013 IEEE International Conference on*. IEEE, 2013, pp. 516–522.

[11] J. A. Newman, "Head injury criteria in automotive crash testing," SAE Technical Paper, Tech. Rep., 1980.

[12] Y. She, H.-J. Su, D. Meng, S. Song, and J. Wang, "Design and modeling of a compliant link for inherently safe corobots," *Journal of Mechanisms and Robotics*, vol. 10, no. 1, p. 011001, 2018.

[13] Y. She, H.-J. Su, C. Lai, and D. Meng, "Design and prototype of a tunable stiffness arm for safe human-robot interaction," in *ASME 2016 International Design Engineering Technical Conferences and Computers and Information in Engineering Conference*. American Society of Mechanical Engineers, 2016, pp. V05BT07A063–V05BT07A063.

[14] A. Stilli, L. Grattarola, H. Feldmann, H. A. Wurdemann, and K. Althoefer, "Variable stiffness link (vsl): Toward inherently safe robotic manipulators," in *Robotics and Automation (ICRA), 2017 IEEE International Conference on*. IEEE, 2017, pp. 4971–4976.

[15] Y. Wei, Y. Chen, Y. Yang, and Y. Li, "A soft robotic spine with tunable stiffness based on integrated ball joint and particle jamming," *Mechatronics*, vol. 33, pp. 84–92, 2016.

[16] J. R. Amend, E. Brown, N. Rodenberg, H. M. Jaeger, and H. Lipson, "A positive pressure universal gripper based on the jamming of granular material," *IEEE Transactions on Robotics*, vol. 28, no. 2, pp. 341–350, 2012.

[17] N. G. Cheng, M. B. Lobovsky, S. J. Keating, A. M. Setapen, K. I. Gero, A. E. Hosoi, and K. D. Iagnemma, "Design and analysis of a robust, low-cost, highly articulated manipulator enabled by jamming of granular media," in *Robotics and Automation (ICRA), 2012 IEEE International Conference on*. IEEE, 2012, pp. 4328–4333.

[18] T. Ranzani, M. Cianchetti, G. Gerboni, I. De Falco, and A. Menciassi, "A soft modular manipulator for minimally invasive surgery: design and characterization of a single module," *IEEE Transactions on Robotics*, vol. 32, no. 1, pp. 187–200, 2016.

[19] M. Henke and G. Gerlach, "On a high-potential variable-stiffness device," *Microsystem technologies*, vol. 20, no. 4-5, pp. 599–606, 2014.

[20] O. Tabata, S. Konishi, P. Cusin, Y. Ito, F. Kawai, S. Hirai, and S. Kawamura, "Micro fabricated tunable bending stiffness devices," *Sensors and Actuators A: Physical*, vol. 89, no. 1-2, pp. 119–123, 2001.

[21] J. L. C. Santiago, I. D. Walker, and I. S. Godage, "Continuum robots for space applications based on layer-jamming scales with stiffening capability," in *Aerospace Conference, 2015 IEEE*. IEEE, 2015, pp. 1–13.

[22] S. Follmer, D. Leithinger, A. Olwal, N. Cheng, and H. Ishii, "Jamming user interfaces: programmable particle stiffness and sensing for malleable and shape-changing devices," in *Proceedings of the 25th annual ACM symposium on User interface software and technology*. ACM, 2012, pp. 519–528.

[23] Y.-J. Kim, S. Cheng, S. Kim, and K. Iagnemma, "A novel layer jamming mechanism with tunable stiffness capability for minimally invasive surgery," *IEEE Transactions on Robotics*, vol. 29, no. 4, pp. 1031–1042, 2013.

[24] G. Zhu, S. S. Ge, and T. H. Lee, "Simulation studies of tip tracking control of a single-link flexible robot based on a lumped model," *Robotica*, vol. 17, no. 1, pp. 71–78, 1999.

[25] S. Kawamura, T. Yamamoto, D. Ishida, T. Ogata, Y. Nakayama, O. Tabata, and S. Sugiyama, "Development of passive elements with variable mechanical impedance for wearable robots," in *Robotics and Automation, 2002. Proceedings. ICRA'02. IEEE International Conference on*, vol. 1. IEEE, 2002, pp. 248–253.